Title:

# Early impairment in dentate pattern separation in a rodent model of temporal lobe epilepsy.

Author list:

**Laura A. Ewell[1,2,3,4], Ario Ramezani[1], Gabrielle Suarez[1], Verónica C. Piatti[1], Vicky Lam[1], Tatyana G. Mills[1], Anelah McGinness[1], Raafat Kuk[1], Mika Ukai[1], Anna-Lena Schlenner[1], Stefan Leutgeb[1,5*], and Jill K. Leutgeb[1,5,6*]**

Affiliations:

[1]Neurobiology Department, School of Biological Sciences, University of California, San Diego, USA

[2]Department of Anatomy and Neurobiology, University of California, Irvine, USA

[3]Department of Neurobiology and Behavior, University of California, Irvine, USA

[4]Center for the Neurobiology of Learning and Memory, University of California, Irvine, USA

[5]Kavli Institute for Brain and Mind, University of California, San Diego, USA

[6]Lead contact

*Correspondence: jleutgeb@ucsd.edu (J.K.L), sleutgeb@ucsd.edu (S.L.)

**SUMMARY**

The dentate gyrus of the hippocampal formation utilizes sparse neural coding to support memory formation. In temporal lobe epilepsy (TLE), the dentate undergoes extensive restructuring, including loss of local inhibition. It is unknown how circuit changes impact dentate network computations in awake behaving animals. Here we perform high-density tetrode recordings from the dentate in male rats treated with systemic kainic acid (KA) to induce TLE. In KA-treated rats, dentate spatial representations were less precise at the single neuron level, however the stability of the spatial code in representing repeated visits to the same location was retained at the population level. Despite spared spatial representation, the network computations for pattern separation were disrupted. The reorganized dentate network in KA-treated rats generated less distinct population activity patterns for different environments, specifically as a result of impaired rate-remapping. Changes in network computations paralleled impairments in a dentate-dependent memory task, potentially providing a link between altered pattern separation and behavioral discrimination. These deficits were present in animals with confirmed dentate circuit reorganization that had not yet developed spontaneous seizures – suggesting that the dentate network changes underlying altered rate-remapping and impaired dentate-dependent memory occur early in epileptogenesis.

**Keywords:** dentate gyrus, medial temporal lobe epilepsy, pattern separation, hippocampus, memory comorbidity

## INTRODUCTION

A critical feature of episodic memory is the ability of neural networks in the hippocampus to represent different events uniquely such that they can be stored and later remembered with minimal interference from memories that share common features. Accurate memory retrieval is thus dependent on encoding memories distinctly when they are formed. The neuronal mechanism proposed to mediate this process is pattern separation, in which the pattern separator receives overlapping input representing similar experiences, and transforms those inputs to non-overlapping, separated outputs such that a memory is represented by a distinct pattern of activity [1-3]. Experimental evidence converges to suggest that the first processing station of the hippocampal trisynaptic circuit, the dentate gyrus, is an optimal pattern separator, confirmed both in rodent models [2,4-7] and in humans [5,8,9]. The dentate gyrus is well positioned to perform this operation based on unique network cytoarchitecture, plasticity, and neuronal activity [10,11]. The dentate gyrus receives dense cortical input from higher cortical areas and sends output (mossy fibers) to the downstream CA3, the auto-associative recurrent network at the core of the hippocampal formation which operates most efficiently for memory encoding when incoming patterns are maximally separated by the dentate gyrus [1,12].

At the heart of the capacity for the dentate gyrus neural network to perform pattern separation is its unique sparsity unlike other neural networks in memory circuits of the brain. An extremely sparse neuronal population code is utilized to separate experiences [13,14,15] . Such sparse activation selection is achieved in part by the large network expansion between the cortex (relatively low numbers of neurons in layer 2 of entorhinal cortex) and the much larger

59 dentate gyrus network [16] . Another essential component is strong feedforward [17] and feedback
60 inhibition [18] that are present within dentate gyrus microcircuits, which effectively silence the
61 majority of neurons, enabling a highly competitive winner take all coding scheme [19] and
62 support sub-second toggling between distinct co-active ensembles [20].

63 Further capacity to generate unique population activity is achieved by combining a
64 distributed cell activation code with a distributed rate code for representing distinct
65 experiences. The active subset of dentate neurons vary their firing rates (rate-remapping) or
66 spatial receptive fields (spatial remapping) to represent different features of similar experiences
67 [2]. These collective neuronal changes magnify memory capacity by expanding the possible
68 unique combinations of neuronal activity at the population level [21,22]. These network dynamics
69 were described in *in vivo* electrophysiological recordings in the dentate gyrus examining the
70 neural mechanism of pattern separation in rodents [2,4,6], and can serve as important windows
71 into memory processes. With this mechanistic understanding, the neuronal mechanisms for
72 pattern separation can be assessed as a readout of proper memory encoding and storage of
73 precise spatial memory.

74 There are several lines of evidence indicating that reduced sparsity in the dentate gyrus
75 weakens pattern separation and leads to memory deficits [23-26]. Perhaps the most significant line
76 of evidence comes from temporal lobe epilepsy (TLE), a disease defined by increased neuronal
77 activity and synchrony, and thus reduced sparsity. Patients with TLE are unable to pattern
78 separate similar visual scenes [27] and mouse models of TLE exhibit reduced *in vitro* dentate
79 pattern separation [28]. Several changes occur in the dentate gyrus network in epilepsy that could
80 account for dentate-dependent memory deficits. Granule cells sprout de novo axons which

create aberrant connections between granule cells [29-31]. Such increased recurrence has been hypothesized to promote hypersynchronous activation of granule cells, promoting pathological high frequency events [32]. Other changes include death of inhibitory interneurons [33,34], which lead to reduced inhibition onto granule cells [35]. Finally, granule cells exhibit changes in dendritic and synaptic properties which alter the plasticity rules of the few active neurons [36,37]. Together, these changes can facilitate overactivation of dentate granule cells [38], which leads to runaway excitation and seizure propagation [39]. It is currently unknown how changes in (1) network recurrence, (2) network inhibition, and (3) seizure burden, impact the neural-network computations in the dentate gyrus that underlie pattern separation and ultimately memory. To address these questions, we first assessed circuit level structural changes and dentate-dependent memory [40,41] in rats with ongoing epileptogenesis prior to seizure generation as well as in rats with chronic epilepsy. At the same time-point in disease progression, we performed high-density single unit recordings from the dentate gyrus in a task where the network mechanisms of pattern separation by place field rate-remapping have been extensively characterized. We report that even prior to developing seizures, rats had impaired dentate-dependent memory. This behavioral deficit emerged at a timepoint when we show that the dentate network experienced loss of inhibitory neurons, altered spatial representations and reduced specificity in the population code via reduced rate-remapping between similar environments.

## RESULTS

102 **Kainic acid induced status epilepticus results in structural changes of the dentate gyrus and**
103 **impaired behavioral discrimination**

104 To test how circuit reorganization in the dentate gyrus network as a result of
105 epileptogenesis and eventually epilepsy impacts dentate-dependent behavior, we induced
106 *status epilepticus* in male rats utilizing the low-dose systemic kainic acid (KA) model while
107 littermates served as controls. Two months after rats were treated with KA, they were
108 continuously video monitored (24 hours a day) for one month to determine disease progression
109 (those with >2 spontaneous behavioral seizures were classified as epileptic) and then were
110 sacrificed for histological analysis. At this timepoint, roughly half of the treated rats were
111 epileptic, which allowed us to track which changes in the dentate gyrus were associated with
112 seizures (epilepsy) versus associated with epileptogenesis. In both control and KA-induced rat
113 populations, we measured two hallmarks of epilepsy that could have direct impacts on dentate
114 network sparsity; mossy fiber sprouting and hilar somatostatin positive (SST+) interneuron cell
115 loss (Figure 1A-D). Mossy fibers are the excitatory output axons of dentate granule cells and
116 SST+ neurons are interneurons that provide feedback inhibition to granule cells. Mossy fiber
117 sprouting was elevated in KA-treated rats that suffered behavioral seizures, but not in those
118 that were seizure free (Figure 1A,C; Figure S1) (ctrl: n = 28 rats, mean ± S.E.M., 0.7 ± 0.1; KA-no
119 seizures: n = 15 rats, 1.1 ± 0.2; KA-seizures: n = 13 rats, 2.1 ± 0.2; one-way ANOVA, df = 2, f =
120 18.6, $p = 7.5 * 10^{-7}$, multiple comparisons: ctrl vs KA-no seizures, n.s., ctrl vs KA-seizures, $p = 3.9$
121 $* 10^{-7}$, seizures vs no seizures, p = 0.0006). We processed a subset of the tissue to stain for SST+
122 neurons. The number of SST+ neurons in the dorsal hilus were reduced in both groups of KA-
123 treated rats, regardless of whether they had yet developed spontaneous behavioral seizures

124 (Figure 1 B,D; ctrl: n = 10 rats, mean ± S.E.M., 2525 ± 271 SST+; KA-no seizures: n = 6 rats, 1183
125 ± 268 SST+; KA-seizures: n = 7 rats, 1371 ± 110 SST+, one-way ANOVA, df = 2, f = 9.52, p = 0.001,
126 multiple comparisons: ctrl vs KA-no seizures, p = 0.005; ctrl vs KA-seizures, p = 0.0009, seizures
127 vs no seizures, n.s.).

128 A subset of the KA induced animals (n = 18) were tested on a dentate-dependent spatial
129 discrimination task during the period that they were being video monitored. In this reference
130 memory task, on each day of training animals choose between two adjacent open arms of an 8-
131 arm radial arm maze, one of which is consistently baited with a food reward (Figure 1E). To
132 confirm dentate dependence of this task, we added an additional group of animals in which we
133 lesioned the dentate gyrus [42]. Dorsal dentate granule cells were selectively lesioned with
134 bilateral infusions of colchicine in the dorsal region of the dentate gyrus of the hippocampus. In
135 the lesioned rats (n = 11), there was a 67.3 ± 4.9% reduction in the volume of the dorsal dentate
136 gyrus granule cell layer, as quantified using the Cavalieri method. We found that lesioning the
137 dentate was sufficient to disrupt learning (requiring more trials to reach criterion) and
138 strikingly, KA-treated rats behaved as poorly as the lesion group (Figure 1F) (ctrl: 70 ± 5 trials, n
139 = 30 rats; KA: 95 ± 10 trials, n = 18 rats; DG Lesion: 105 ± 15 trials, n = 11, one-way ANOVA, df =
140 2,f = 6.27, p = 0.003; multiple comparisons: ctrl vs KA, p = 0.03, ctrl vs lesion, p = 0.009, KA vs
141 lesion, p = 0.7). Within the KA group, there was no behavioral difference between KA animals
142 with or without seizures (seizures: 110 ± 20 trials, n = 7 rats; no seizures: 90 ± 10 trials, n = 11,
143 unpaired t-test, t = 1.19, df = 16, p = 0.25), suggesting that brain changes associated with
144 epileptogenesis were sufficient to disrupt dentate-dependent memory. Collectively, these data
145 imply that early changes to the dentate gyrus network during disease progression, i.e. before

146 the emergence of the spontaneous seizures that define epilepsy, are sufficient to alter the
147 network computations necessary to support behaviors that require fine spatial discrimination.

148

149 **Impaired spatial information and reduced spatial sparsity in the neural activity of KA-treated**
150 **rats**

151 To link how disease related circuit reorganization in the dentate gyrus resulted in
152 altered dentate-dependent memory we next focused on characterizing changes in dentate
153 network activity in KA treated rats. We first asked whether structural changes such as loss of
154 inhibition and increases in excitatory connectivity in epileptogenesis are accompanied by
155 physiological changes in dentate neurons in awake-behaving rats. We recorded activity from
156 dentate principal neurons while rats explored distinct spatial environments, a condition where
157 dentate neurons in the healthy brain were previously shown to represent different
158 environments with unique firing patterns [2,4,6]. Rats were trained to forage for food in open-field
159 environments that differed in shape (Ctrl: n = 39 neurons, n = 6 rats; KA: n = 60 neurons, n = 6
160 rats). We tested whether there were general differences in dentate cellular excitability between
161 control animals and those that had undergone KA induced *status epilepticus* 2 months prior.
162 Distributions of peak firing rates during foraging were similar between the two groups (Median,
163 IQR; Ctrl: 2.2 Hz, 0.3 - 5.6 Hz; KA: 2.0 Hz, 0.5 - 7.8 Hz). Neurons with peak firing rates >2 Hz were
164 considered active during foraging and comprised a similar proportion of total neurons in control
165 and KA-treated rats (Ctrl, n = 22 neurons or 56%; KA, n = 30 neurons or 50%; Figure 2B). Of the
166 active neurons (>2 Hz), KA-treated dentate neurons had similar average firing rates (M, IQR: 0.9

167 Hz, 0.6 - 1.7 Hz) compared to control neurons (M, IQR: 0.3 Hz, 0.2 - 0.6 Hz; p = 0.13, rank-sum;
168 z-val: -1.5; Figure 2C). Despite similar firing rate distributions, we observed differences in the
169 spatial receptive fields of active cells, measured by assessing the quality of their spatial
170 representations while rats explored the open field. In control rats, even neurons with low
171 spatial information scores (a measure of how well a neuron's firing rate predicts the rat's
172 position) exhibited well defined place fields, the difference to higher scores being that cells with
173 lower spatial information had multiple rather than single well defined firing fields within the
174 same environment (Figure 2D, left, bottom row). In contrast, in KA-treated rats, cells had spatial
175 information scores that were below the control range and the cells with the lowest scores were
176 characterized by distributed firing patterns such that the neurons fired across most spatial bins
177 in the open-field (Figure 2D, right, bottom row). In line with this observation, across the
178 population of active neurons, spatial information was lower in KA-treated rats (M, IQR: 0.8, 0.4
179 - 1.7) compared to control rats (M, IQR: 1.8, 1.2 - 2.2; p = 0.0056; rank-sum, z-val: 2.8; Figure 2E,
180 left). Furthermore, we observed differences in spatial non-selectivity (a measure of the
181 proportion of spatial bins within the environment that the neuron was active in). Across the
182 population, KA-treated dentate neurons exhibited higher spatial non-selectivity (KA-treated
183 neurons: M, IQR, 0.42, 0.19 - 0.60 compared to control neurons: M, IQR, 0.19, 0.15 - 0.29; p =
184 0.017, rank-sum, z-val: -2.4; Figure 2E, right). These results confirm that the spatial firing
185 patterns of dentate neurons following epileptogenesis are altered despite retained average
186 firing rates. Together, the reduced spatial information and increased spatial non-selectivity
187 indicate that in KA-treated rats, at each location within an open-field, a higher number of
188 dentate neurons are active. Therefore, during an experience at any given moment in time, the

189 dentate network is indeed less sparse in KA-treated rats in comparison to controls. We
190 observed behavioral seizures (Racine III-V) in four of the six KA-treated rats (4 hrs/day of video
191 monitoring, see methods for more details). We therefore asked whether the observed changes
192 in place field quality were driven by neurons recorded in animals with observed behavioral
193 seizures. When testing between neurons recorded from KA-treated rats with seizures (n = 17)
194 vs. without seizures (n = 13), we found no differences in average firing rate (with seizures: 0.6,
195 0.3 - 1.6; without seizures: 0.3, 0.2-1.2, rank-sum, p = 0.4, z-val:-0.8; Figure S2A), spatial
196 information (with seizures: 0.8, 0.4 – 1.7; without seizures: 0.8, 0.6-1.3, rank-sum, p = 0.77, z-
197 val: 0.29; Figure S2B), or spatial non-selectivity (with seizures: 0.5, 0.2-0.7, without seizures:
198 0.4,0.3-0.5, rank-sum, p = 0.62, z-val: -0.5; Figure S2C), suggesting changes in neuronal firing
199 patterns occurred prior to seizure generation. We therefore pooled all KA-treated animals for
200 further electrophysiological analysis.

201 One feature of neurons in the dentate gyrus is that individual place cells often have
202 many distinct spatial firing fields. Multiple place fields per cell endow the sparse network with
203 the capacity to create as many distinct population codes with fewer active cells as a much
204 larger network of active cells can generate from fewer place fields per cell [2]. We observed that
205 the number of fields per neuron and the size of fields were not statistically different between
206 control and KA-treated rats (Figure 2F). Note, however, that we observed a skewed distribution
207 for number of fields in dentate neurons recorded in KA-treated animals, with a quarter of cells
208 having >5 fields. KA-treated rats had significantly higher within field mean firing rates,
209 unmasking a hyperexcitability phenotype that was occluded when considering overall activity
210 (ctrl: n = 24 fields, 2.3 ± 0.3 Hz; KA: n = 55 fields, 3.1 ± 0.2 Hz, rank-sum, z-val = -2.4, p = 0.014;

211 Figure 2F, right). Collectively we observed several features of altered dentate neuronal activity
212 in KA-treated rats that suggests reduced network sparsity manifests early in disease progression
213 before seizures emerge. These results are in line with our observation that dentate-dependent
214 memory impairments were also present in animals treated with KA, but prior to the emergence
215 of behavioral seizures.

216

217 **Dentate network computations that encode and represent events distinctly are impaired in**
218 **KA-treated rats**

219 An important neural-network computation of the dentate gyrus is to distinguish
220 between similar input patterns, or events, by generating distinct population activity for each
221 input that can then be conveyed to downstream hippocampal subregions that are not
222 optimized for pattern separation [2,43]. Pattern separation is considered a critical network
223 computation for the encoding of memory that facilitates accurate memory retrieval. To
224 differentiate between environments, dentate neurons either change their spatial firing fields,
225 in-field firing rates, or turn on/off such that the neural representations of similar environments
226 are strongly decorrelated from one another at the population level [21,44]. To test whether
227 dentate network computations for pattern separation were altered in KA-treated animals, we
228 trained rats to explore an open field arena with flexible walls that could be in either a square or
229 circular configuration (Figure 3A). The arena remained in the same spatial location in the room,
230 with walls placed upon the same section of floor leaving the majority of distal and proximal
231 cues unchanged between trials except for the shape of the enclosure walls. Trials consisted of

232 four ten minute-sessions in which box shape varied between a square or circle randomly. This
233 design allowed us to test pattern separation by comparing dentate population activity in the
234 same location between visits when the same environmental cues were repeated (same shape)
235 and when the environmental cues differed (different shape) (Figure 3B).

236 To make these comparisons, we constructed population vectors that allow for testing of
237 dentate network decorrelation between environments. Population vectors include both the
238 spatial aspect (where in the environment the neurons are active) and the rate aspect (the
239 magnitude of the activity in each spatial bin) for the entire population of active cells in the
240 network [21] (Figure 3C). Place maps from each neuron were generated for each of the four
241 sessions (i.e., two for each of the two environment shapes). The maps of neurons that were
242 active in at least one of the shapes were stacked into a 3-dimensional matrix with x and y
243 corresponding to matching spatial bins and z corresponding to cell identity. Pairs of vectors for
244 each spatial bin(x,y), comprising the average rate for every neuron within that bin, were
245 correlated across either maps from the same shapes (square-square, circle-circle) or different
246 shapes (square-circle). First, we confirmed previous results [2] for dentate network computations
247 in control animals (Figure 3D). In control, same shape PV correlations were high, reflecting the
248 same population activity in repeated visits to the same locations (correlation = 0.79 ± 0.009). As
249 expected, different shape comparisons plunged to low correlation values reflecting different
250 patterns of activity associated with different environments (correlation = 0.31 ± 0.01, reduced
251 by 0.48 ± 0.01). In KA-treated rats, same shape PV correlations were also high (correlation =
252 0.82 ± 0.01), but were reduced to a lesser extent across different shapes (correlation 0.57 ±
253 0.01, reduced by 0.25 ± 0.01, $p = 5 * 10^{-61}$, unpaired t-test; t stat: 17.05). Thus, the

254 discrimination of different environmental cues was diminished for dentate networks of KA-
255 treated rats compared to control rats.

256 Next, we further explored the nature of the network discrimination deficits in KA-
257 treated rats to determine whether changes in spatial representations or rate distributions were
258 differentially affected in the KA-treated dentate network. Spatial correlations between the
259 place maps generated from active dentate neurons across same-shape comparisons (circle-
260 circle and square-square) were high for control and KA-treated rats, indicating robust stability
261 of spatial representations for both groups (mean ± S.E.M.; Ctrl: n = 36 comparisons, 0.69 ± 0.04;
262 KA: n = 40 comparisons, 0.57 ± 0.05). Furthermore, a correlation of place cell maps between
263 different environments yielded significantly lower values than for the across-shape comparison
264 for both groups (one-way ANOVA, df = 3, f = 17.39, $p = 3.2 * 10^{-10}$, $p<0.001$, post-hoc Tukey-
265 Cramer correction for group comparisons, mean ± S.E.M.; Ctrl: n = 76 comparisons, 0.31 ± 0.03,
266 $p = 4.0 * 10^{-8}$; KA: n = 86 comparisons, 0.31 ± 0.04, $p = 4.0 * 10^{-4}$; Figure 3E, left). In contrast to
267 the similar response of spatial representations in control versus KA-treated rats, we observed a
268 difference in rate discrimination by place fields (Figure 3E, right). Note that rate analyses were
269 done on individual place fields rather than the full spatial map of an environment to account for
270 the independent rate code of individual firing fields that have been shown to represent changes
271 in non-spatial cues across environments [2]. In control rats, the firing rates within place fields
272 were similar between visits to the same environment, but more distinct between visits to
273 different environments, as would be expected when changes in rate is used to discriminate
274 between different environmental cues (reduction of 0.3 ± 0.05, n = 24 fields, sign-rank, z-val =
275 4.01, $p = 5.9 * 10^{-5}$). KA-treated rats also exhibited a higher rate difference between different

276 compared to same environments (reduction of 0.12 ± 0.04, n = 55 fields, sign-rank, z-val = 2.1, p
277 = 0.03). However, the magnitude of the rate change between same vs. different was
278 significantly larger in controls compared to KA-treated rats (rank-sum, z-val = 3.2, p = 0.0013).
279 Taken together, our results suggest that pattern separation supported by a redistribution of
280 firing rates, a mechanism for the generation of unique population codes for distinct events, is
281 selectively more sensitive to changes in the dentate network as a result of epileptogenesis.

282

283 **DISCUSSION**

284 The dentate gyrus undergoes massive restructuring in TLE, yet there have been few studies
285 examining how neural network computations of the dentate gyrus may or may not be
286 compromised. In line with previous work, we observed two histological changes in the dentate
287 gyrus with the induction of epileptogenesis – sprouting of recurrent granule cell axons and loss
288 of somatostatin interneurons – both of which would be predicted to lead to hyperexcitability of
289 dentate gyrus neurons and a loss of network sparsity. In parallel we observed a deficit in
290 dentate-dependent memory along with the degradation of neural-network computations
291 essential for the dentate gyrus contribution to memory encoding. Epileptogenesis induced
292 impairment in the spatial coding features of individual dentate neurons including less precise
293 spatial firing with higher within field firing rates. However, despite a less precise spatial
294 representation at the single neuron level, the stability of the spatial code for repeated visits to
295 the same environment was retained at the population level. The degraded pattern separation
296 in the dentate networks of KA-treated rats for representing distinctly different environments

297 was instead a result of reduced rate-remapping that impaired the capacity of the reorganized
298 dentate network to generate distinct population patterns needed to distinguish between
299 similar familiar environments, which may in turn preclude the cueing of accurate memory
300 retrieval in downstream neural networks.

301 In our experiments, KA-treated rats showed interneuron loss, behavioral deficits, and
302 impaired pattern separation in the dentate even if they had not yet developed the spontaneous
303 behavioral seizures that define epilepsy. These results suggest that dentate specific memory
304 deficits such as learning to discriminate adjacent spatial locations may be an early
305 manifestation of epileptogenic circuit changes that impair select dentate network computations
306 prior to the development of spontaneous seizures. The timeline in dentate may be different
307 than in other regions of the hippocampus. For example, in CA1, it has been reported that place
308 field spatial information reduced concurrently with the progressive increase in spontaneous
309 seizure frequency and that reductions in spatial stability emerged weeks later [45]. Earlier
310 impairments in dentate function may provide a biomarker for assessing the risk for developing
311 acquired epilepsy after brain injury or stroke. Indeed, epileptic patients clearly exhibit impaired
312 pattern separation [27,28], although to our knowledge no longitudinal study has been done to
313 assess whether performance on such tasks predict disease outcomes.

314 An early feature of epileptogenesis is interneuron loss in the hippocampus [46]. Specific to
315 the dentate gyrus, loss of interneurons in the hilus has been widely reported [35,47]. Even though
316 remaining interneurons sprout, they are unable to compensate, resulting in a net loss of
317 inhibition to the dentate network [48]. Confirming these reports, we also report a loss of
318 interneurons in the dentate hilus – specifically SST+ containing interneurons (Figure 1D). It is

319 interesting to consider how this early circuit change may be linked to the altered physiology we
320 observe. Lateral inhibition has been shown to exert a critical circuit level constraint on the
321 number of neurons active at a particular location [49,50], which may explain the reduced spatial
322 selectivity we observed in neurons recorded from KA-treated rats. SST+ interneurons are also
323 known to regulate spike bursting within place fields [51]. Consistent with this role, we observed
324 increased mean firing rate within fields (Figure 2F). The early influence of SST+ cell loss on
325 network rate-remapping could be a combination of both direct effects of the reduced inhibition
326 on select cortical inputs to dentate, as well as the broader effects of reduced inhibition on
327 dentate network sparsity.

328 Dentate network sparsity is hypothesized to play a critical role in setting the level of
329 pattern separation that can be achieved through unique combinations of population activity [14].
330 The fewer neurons capable of overcoming the strong inhibition characteristic of a competitive
331 network like the dentate gyrus [19], the more unique patterns of activity can be achieved from
332 the total number of dentate neurons. The possible number of unique population codes is
333 hypothesized to be directly related to the memory capacity of the hippocampus [1,12]. Moreover,
334 it has been shown experimentally that directly altering the inhibitory gain of the dentate
335 network through the loss of other inhibitory cells results in more neurons becoming active for a
336 given input representation (reduced sparsity) and impaired pattern separation [52,53]. However,
337 the loss of SST+ interneurons could have a more direct influence on rate-remapping, the
338 identified network computation selectively impaired early in epileptogenesis while spatial
339 coding is retained. Somatostatin interneurons inhibit the distal dendrites of dentate granule
340 neurons in the outer molecular layer [54]. The outer and inner molecular layers are defined by

341 select cortical inputs that terminate on distinct regions of dendrite. Input from the lateral
342 entorhinal cortex (LEC) reaches granule neurons via the lateral perforant path, terminating on
343 the distal dendrites of granule neurons where SST+ interneurons regulate activity [55]. Input from
344 the LEC has been shown to convey mainly nonspatial information to hippocampus [56,57] and to
345 be necessary for rate-remapping to occur in CA3 neural-networks under the same behavioral
346 conditions tested here [58]. These results suggest that a select disruption of LEC inputs to dentate
347 gyrus via a reduction in SST+ inhibition could also result in impaired rate-remapping with a
348 preservation of the spatial code from medial inputs. Although direct tests are needed to reveal
349 longitudinal timelines and include causal manipulations, our results suggest a direct link
350 between SST+ loss and an early impairment in dentate network computations for memory
351 rather than spatial coding, providing a therapeutic target for early intervention and the
352 potential rescue of memory comorbidities.

353 The second histological feature we considered as an early feature of epileptogenesis in
354 the hippocampus was mossy fiber sprouting. We only observed significant levels of sprouting in
355 animals in which we observed spontaneous seizures. The link between sprouting and
356 pathological population bursts in the dentate has been previously reported [29,59]. Our data
357 suggest that mossy fiber sprouting is better associated with seizure outcomes and is preceded
358 by changes to dentate network computations and dentate-dependent memory deficits. Our
359 findings do not preclude the possibility that sprouting and seizure activity would not further
360 exacerbate cognitive problems. In fact, seizure activity has been shown to impact hippocampal
361 neuronal activity and network computations in additional ways, included changes in spatial
362 information processing [60 61] . These results highlight that the disease progression that leads to

363 dentate dependent memory problems versus seizure susceptibility are on separate trajectories
364 and may not share common mechanisms.

365 Together, these data highlight the importance of the dentate gyrus for pattern
366 separation and underscore its dysfunction in TLE cognitive comorbidities. Impairments in
367 dentate physiology emerge before spontaneous seizures, indicating that functional assessment
368 of dentate memory could be a powerful biomarker for determining disease outcomes. Testing
369 pattern separation in humans has been done at both the imaging and behavioral level [5,8,9],
370 further motivating the therapeutic importance for our finding that pattern separation
371 computations in the dentate gyrus are early outcomes of epileptogenesis and precede seizure
372 outcomes. These results also point to a fundamental role of inhibition in the dentate network
373 for supporting its function – indicating that interneuron transplant therapies [62], which have had
374 success in treating cognitive comorbidities after brain injury could be an exciting avenue for
375 dentate-dependent memory in TLE as well [63].

376

377 **Acknowledgements**: We thank M. Wong, Y. An, M. Appalaraju, and M. Andersson for technical
378 assistance. This work was supported by the Hellman Foundation, Epilepsy foundation grant
379 157927, NIMH grant R01MH119179, and the Walter F. Heiligenberg Professorship to J.K.
380 Leutgeb; NIH grants R01 NS102915, R21 MH100354, R01 NS084324, and R01 NS097772 to S.
381 Leutgeb. L.A. Ewell was supported by NIH training grant F32MH096526.

382

**Author Contributions**: L.A.E., S.L. and J.K.L. conceived experiments, designed study, and interpreted data. S.L. and J.K.L. managed the project. L.A.E., with assistance from L.M., T.G., and A-L.S, performed electrophysiological experiments. L.A.E., G.S., and A.M. scored seizure monitoring, G.S. and A.M. performed immunohistochemistry and microscopy, V.P. provided dentate lesion data, and A-L.S. quantified the lesion data. L.A.E., G.S., A.M., R.K., and M.K. performed behavioral experiments. L.A.E. analyzed data and prepared figures. L.A.E. prepared the manuscript with feedback and editing from J.K.L. and S.L.

**Ethics Declarations**: The authors declare no competing financial interests.

392 **METHODS**

393 **Subjects**

394 All experimental procedures were performed as approved by the Institutional Animal Care and
395 Use Committee at the University of California, San Diego and according to National Institutes of
396 Health and institutional guidelines. Epilepsy was induced as in previous studies [64 61] using a
397 repeated low-dose kainate chronic model of temporal lobe epilepsy [65]. Male Long Evans rats (n
398 = 52, 40 days of age, Charles River, CA) were treated with kainic acid (KA) (5 mg/kg, i.p., Tocris)
399 each hour until the onset of status epilepticus, which was defined as >10 motor seizures per
400 hour of class IV or V on the Racine scale [66]. After the seizure induction protocol, the rats were
401 housed individually and maintained on a reverse 12 hr light/12 hr dark cycle. To confirm
402 whether chronic spontaneous seizures that define epilepsy had developed, rats were video-
403 monitored for 4 hours per day for electrophysiological studies or 24 hours per day for
404 behavioral and histological studies. Once two or more motor seizures of class III or greater on
405 the Racine scale were observed, the animal was considered epileptic. Twenty-eight KA-treated
406 rats (3.5 – 4.5 months old) were continuously video monitored for 1 month and paired with 28
407 control rats not injected with KA (4 months old), after which they were sacrificed for
408 histological analysis of circuit reorganization. Six KA-treated rats (6-12 months old) and six
409 control rats not injected with KA (6 -12 months old) were used for electrophysiological
410 experiments. Two of the control rats used for electrophysiological experiments were wildtype
411 GFAP-TK rats on a Long Evans background [67]. Eighteen KA-treated rats (6-8 months old) and 30
412 control rats not injected with KA (6-8 months old) were used for behavioral experiments.
413 Eleven wildtype GFAP-TK rats on a Long Evans background were injected with colchicine to

414 lesion the dentate gyrus and were used for behavioral experiments. The transgenic GFAP-TK rat
415 line was originally provided by Dr. Heather A. Cameron (National Institutes of Health) and
416 maintained by breeding with wildtype Long Evans rats obtained from Charles River Laboratory.

417

418 **Surgical procedures - chronic electrophysiological recording device**

419 Rats were anesthetized with isoflurane (2% to 2.5% in $O_2$) and an electrode assembly
420 (Hyperdrive, designed by the McNaughton laboratory [68]) comprising 14 independently movable
421 tetrodes was implanted above the right hippocampus (AP, 4.1 mm posterior to bregma; ML, 3.0
422 mm) and fixed to the skull using stainless steel screws and dental cement. Two screws were
423 used as animal ground and were implanted to touch the surface of cortex, anterior and lateral
424 to bregma. Tetrodes were prepared by twisting four insulated platinum wires together
425 (diameter = 0.017 mm, California Fine Wire Company). Leads were plated with platinum prior
426 to surgery to obtain stable impedances near 200 kOhm. Two tetrodes had all four leads shorted
427 with one of the two left in the cortex to record a differential reference signal, while the other
428 was advanced to stratum radiatum to record local field potentials (LFP). The other 12 tetrodes
429 were positioned in the dentate gyrus cell layer to record single units.

430

431 **Tetrode recording locations**

432 Histological sections through segments of the hippocampus with electrode tracks were
433 collected as described below (see Histology section). All tetrodes of the 14-tetrode bundle were

434 identified by matching tetrode positions in the bundle with electrode tracks (small lesions) in
435 postmortem tissue. Recordings from a tetrode were included in the data analysis if the
436 tetrode's deepest position could be clearly identified within or adjacent to (touching) the
437 dentate gyrus granule cell layer (see Figure 2A).

438

439 **Surgical procedures - dentate gyrus lesions**

440 Dentate gyrus lesions were performed as described previously [69]. At the time of surgery, the rat
441 was anesthetized with isoflurane gas [2- 2.5% in $O_2$ (20 mL /1 L per minute)] and buprenorphine
442 (0.05 mg/kg, s.c.) was given as an analgesic. To create a lesion specific to granule cells of the
443 dorsal dentate gyrus, colchicine (2.5 mg/ml in 0.1M phosphate buffer, pH 7.2) was injected into
444 3 sites (0.04 µl per site at 0.012 µl per minute) in both hemispheres at the following coordinates
445 anterior-posterior, medio-lateral from bregma and ventral from dura (in mm): (1) -2.8, ± 0.9, -
446 3.7 (2) -4.0, ± 2.1, -3.6, (3) -5.2, ± 3.2, -3.7. Three animals received injections only at sites (1)
447 and (2). Infusions were made using a 1 µl Hamilton syringe and the needle was left in place for
448 8 min at each injection site to prevent spread. Colchicine has previously been shown to cause
449 selective cell death of dentate granule cells [70 71]. Using computer-based 3D volumetric analysis,
450 the volume of the dorsal dentate gyrus granule cell layer and dorsal CA1 and CA3 pyramidal cell
451 layers was quantified in cresyl violet stained, 40 µm thick brain sections. To assess the
452 completeness of the dorsal dentate gyrus lesions and to assess damage outside the dentate
453 gyrus, the Cavalieri estimator in the Stereo Investigator software (grid size 20 µm; 10x
454 objective) was used for volume quantification. The remaining granule cell volume was

455 normalized to a control volume of 1.54 * $10^9$ $\mu m^3$ (n = 3 rats). The remaining granule cell
456 percent volume was low and comparable in the two dorsal hemispheres (left: 29.9 ± 4.7 %
457 remaining, right: 35.4 ± 5.7 % remaining). Only minor mechanical damage was observed in the
458 CA1 region above the dentate injection site. Similar damage was previously shown to not
459 significantly contribute to dentate-dependent memory impairment [69], or an impairment in CA1-
460 dependent memory [40].

461

462 **Recordings and data acquisition**

463 Single units and LFP were recorded during restful and running behavior using a data acquisition
464 system (Digital Lynx SX; Neuralynx) with 64 digitally programmable amplifiers. Unit activity was
465 amplified and band-pass filtered between 0.6 and 6 kHz. Spike waveforms above a trigger
466 threshold (40 µV) were time stamped and digitized at 32 kHz for 1 ms. The LFP was recorded
467 continuously in the 0.1 - 900 Hz band from one of the wires of each tetrode. All recording
468 sessions occurred during the animal's dark cycle (between 7 am - 7 pm). Rats were food
469 deprived to 85% of their baseline weight and trained to forage for randomly scattered food
470 reward (chocolate cereal crumbs) in open arenas. Open arenas were enclosed by a set of
471 flexible walls that could either be in a circular formation (diameter = 1.0 m, height = 0.5 m) or a
472 square formation (0.8 × 0.8 m, height = 0.5 m). Behavioral sessions consisted of four 10 min
473 foraging epochs preceded and followed by resting periods. The rats were also allowed to rest in
474 a holding box for 5 min between foraging epochs. For position tracking, light emitting diodes on
475 the head-mounted preamplifier were tracked at 30 Hz by processing video images.

476 **Cell clustering**

477 Single units were manually sorted using MClust (MClust 3.5, written by A. David Redish;
478 http://redishlab.neuroscience.umn.edu/MClust/MClust.html) adapted to aid in the tracking of
479 cell identity over extended periods of time [72]. Clusters that persisted in the same region of
480 parameter space throughout a behavioral session were accepted for analysis, such that the
481 action potentials of a given neuron included in the analysis did not change shape, were distinct
482 from noise signals, and remained inside the cluster boundary. The cluster was required to be
483 clearly defined in both the first and last rest period of the recording session, but was not
484 required to be present in individual foraging epochs, as many dentate gyrus single units are
485 silent within a particular environment.

486

487 **Neuronal firing rate map**

488 For each neuron, we constructed firing rate maps for each behavioral session by summing the
489 total number of spikes that occurred in a given location bin (5 × 5 cm), dividing by the total
490 amount of time that the rat occupied the bin, and smoothing with a 5 × 5 bin Gaussian filter
491 with a standard deviation of approximately one bin:

492 [0.0025 0.0125 0.0200 0.0125 0.0025;
493 0.0125 0.0625 0.1000 0.0625 0.0125;
494 0.0200 0.1000 0.1600 0.1000 0.0200;
495 0.0125 0.0625 0.1000 0.0625 0.0125;
496 0.0025 0.0125 0.0200 0.0125 0.0025].

Bins that were never within a distance of less than 2.5 cm from the tracked path or with total occupancy of less than 150 ms were regarded as unvisited and were not included in the rate map. Spatial firing patterns of individual cells were compared between sessions when that cell was active (>2 Hz in at least one of the sessions). For each cell, the comparison was performed by calculating the Pearson correlation coefficient for firing rates in corresponding spatial bins across pairs of spatial maps.

**Active neurons**

The total number of single units was determined as the number that were tracked across resting and foraging behavior. All included single units were active during the first and last resting period (validating their stability), but not all single units had high firing rates during foraging epochs. Thus, we determine the proportion of active neurons in behavior as the number of neurons that had at least one neuronal firing rate map with a peak >2 Hz divided by the total number of single units recorded (neurons that were clearly isolated and active in sleep sessions before and after running sessions).

**Spatial information score**

Spatial information was calculated for each neuron for each foraging session in which the neuron had a peak firing rate of at least 2 Hz in at least one spatial bin. We calculated the spatial information per spike for each firing rate map as: $I = \sum_i P_i \frac{R_i}{R} log_2 \frac{R_i}{R}$ where *i* indexes

517 the spatial bins, $P_i$ is the probability of occupancy in each bin, $R_i$ is the mean firing rate in each
518 bin, and R is the mean firing rate across the spatial map [73].

519

520 **Place field boundaries**

521 Individual spatial firing fields of neurons were isolated as previously described [72]. A reference
522 map was calculated as the average of the common area of the four rate maps corresponding to
523 the four behavioral sessions. For each firing peak in the rate map (>0.8 Hz), contours were
524 calculated at 20 levels between zero and the peak rate. For overlapping contours between
525 fields, each shared contour was divided into segments at inflection points of the contour, and
526 each segment was assigned to the nearest field. After fields were determined, only fields with
527 peak rates >2 Hz and at least 50 $mm^2$ were included for further analysis.

528

529 **Population vector correlations**

530 For each behavioral session, rate vectors were constructed by arranging the spatial maps of all
531 cells recorded from that region from all animals in an x-y-z stack, where x and y represent the
532 two spatial dimensions and z represents the cell-identity of the population [44] [21]. To allow for
533 comparisons between the square and circular enclosure shapes, the analysis was restricted to
534 the 16 by 16 bins that were common to both shapes, yielding 256 x-y locations. Population
535 vector correlations were obtained by calculating, for each x-y location, the Pearson correlation
536 coefficient for firing rates along the z-dimension between pairs of sessions. Cells with firing

below 2 Hz in all x-y bins of the two sessions that were compared were excluded from the population vectors before calculating the correlation coefficients. The correlation coefficients from same shape comparisons (circle-circle and square-square) of all spatial bins were averaged to estimate the population vector correlation for a pairwise comparison between same sessions. The average same shape correlation was subtracted from each different shape comparison correlation to quantify the extent of decorrelation in distinct environments.

**Dentate-dependent behavior**

We adopted a behavioral discrimination task that is dependent on the dentate gyrus. Rats learned to discriminate between adjacent arms on an 8-Arm Radial Maze [42]. The maze was in a room with spatial cues on the walls (not on the maze). The maze was comprised of 8 arms arranged around an octagonal stem. Each arm was spaced 45 degrees apart from its adjacent arms. The maze measured approximately 188 centimeters in diameter and was elevated approximately 36 centimeters above the ground. Transparent Plexiglas walls were placed around the central stem of the maze and attached with Velcro in order to block unused arms and designate the two arms that were open per trial. For the adjacent arm discrimination task open arms would either be arm 1 and 2 or arm 1 and 8. Uniform, chrome, silver bowls were taped to the end of each arm. The bowl of the reward arm (arm 1) was the location of the food reward (chocolate cereal) for all behavior testing performed during this experiment. Rats were food restricted to 85% of their baseline weight and maintained at that weight for the duration of habituation and testing. Habituation was conducted in three phases. The first phase involved

558 placement of a single food reward at the stem of the maze, midway down the three
559 experimental arms, just outside the silver bowls, and inside each bowl. The animal was given 10
560 minutes to explore during this phase of habituation. If all 10 rewards were eaten within the 10-
561 minute time frame, the rat moved to phase 2. For phase 2, reward was placed within the bowls
562 and just outside the bowls of the same three arms. Eating all rewards within 10 minutes
563 allowed the rat to pass to phase 3, in which reward was only in the three bowls. Rats had 5
564 minutes to eat all rewards to move onto testing. During testing, the rat ran 10 trials per day. For
565 each trial two adjacent arms were open (1 and 2) or (1 and 8). Each adjacent, non-rewarded
566 arm was used 5 times among the 10 trials in a pseudo-random order to ensure that the rat was
567 not relying on a right-left strategy when making its decision. Reward was always at arm 1. For
568 each day, the number of correct trials were counted. In between trials, the rat was enclosed
569 under an opaque bucket in the central stem. All arms were washed with water and dried
570 between trails. Testing continued until the rat reached a criterion of 90% correct trials for 2 of 3
571 consecutive days, or for a maximum of 17 days. The total number of trials to reach criterion
572 were summed. Initially, behavioral testing was done in rats that were not monitored 24 hours
573 for behavioral seizures. The behavioral performance of non-monitored KA-treated animals did
574 not differ from video-monitored KA-treated animals (non-monitored: 90 ± 10 trials, n = 8 rats;
575 monitored: 95 ± 10 trials, n = 18 rats; unpaired t-test, t = -0.45, df = 24, p = 0.66), therefore data
576 were pooled. Among monitored KA-treated animals, those that had seizures had similar
577 performance to those who did not (seizures: 110 ± 20 trials, n = 7 rats; no seizures: 90 ± 10
578 trials, n = 11; unpaired t-test, t = 1.19, df = 16, p = 0.25), therefore data were pooled. Control
579 animals from lesion experiments were 5 months old, while control animals from epilepsy

580 experiments were 6 months old. No statistical difference in behavioral performance was
581 observed between control groups (epilepsy control: 70 ± 5 trials, n = 21 rats; lesion control: 60 ±
582 5 trials, n = 9 rats; unpaired t-test, t = 1.18, df = 28, p = 0.25), therefore data were pooled.

583

584 **Histology**

585 The rat was deeply anesthetized with isoflurane and given a lethal injection of Pentobarbital
586 (0.8 mL - 2 mL). Rats were systemically perfused, first with 0.37% sulphide solution and then
587 with 4% paraformaldehyde (PFA). Brains were transferred to 30% sucrose in 1X PBS before
588 sectioning with a frozen microtome (40 µM sections, Leica).
589 *Somatostatin immunohistochemistry:* Every sixth, coronal section (40 µm) was processed for
590 staining. Sections were washed (3 x 5 min) in 1X PBS. The free-floating sections were then
591 blocked for 1 hour in blocking solution at room temperature (10% horse serum (HS)
592 and 0.3% Triton-X in PBS). After blocking, the sections were incubated in diluted 1:300
593 monoclonal mouse anti-somatostatin antibody (GeneTex, code GTX71935, clone SOM-018)
594 with 10% HS and 0.3% Triton-X in PBS over two nights at 4$^{o}$C. After washing (3 x 5 min) in 1 x
595 PBS, the sections were then incubated for 1 hour at room temperature in diluted (1:200)
596 biotinylated horse anti-mouse IgG antibody (Vector BA-2000) with 0.3% Triton-X in PBS, and
597 then washed again. Endogenous peroxide activity was blocked with 0.3% $H_2O_2$ for 30 minutes at
598 room temperature. The sections were washed again and then incubated with the avidin-biotin-
599 peroxidase technique (Vectastain ABC Kit, Vector Labs, USA) for 30 minutes at room
600 temperature. The complex was developed using 0.05% of 3,3'-diaminobenxidine (DAB)

601 tetrahydrochloride, 0.3% $NiCl_2 \cdot 6H_2O$ stock, and 0.05% hydrogen peroxide as a substrate
602 for the peroxidase reaction. The sections were then mounted onto Fisherbrand Superfrost Plus
603 Microscope Slides. Stereology of the SST-immunostained tissue was performed using a Leica
604 CTR 6000 microscope and the optical fractionator method and the Cavalieri principle on Stereo
605 Investigator 10 (MBF Bioscience). The counting frame was 300 μm × 300 μm and the counting
606 grid was also 300 μm × 300 μm. After counting SST interneurons in the dorsal hilus of each rat,
607 the total SST interneuron population was estimated based on the thickness of the mounted
608 sections (40 μm).
609 *TIMM staining:* Sections were mounted onto Fisherbrand Superfrost Plus Microscope Slides
610 with a gelatin and PBS mounting solution and left to dry overnight. Slides were placed in
611 distilled water for 3 minutes and then incubated in developer solution in the dark. The
612 developer solution is: 120 mL of Gum Arabic (100 g/200 mL), 10 mL of filtered citrate buffer
613 (51g $C_6H_8O_7$/200 mL; 47g $C_6H_5Na_3\text{-}O_7$ - $2H_2O$/200 mL), 60 mL of 1.7% hydroquinone solution,
614 and 1 mL of 0.09% light-sensitive, silver nitrate solution. After 30 minutes of incubation, the
615 developer solution was mixed and the tissue was re-submerged for at least another 30 minutes.
616 If the stain was not dark enough, the tissue was left in solution until the stain was complete.
617 The slides were then dipped twice in warm distilled water (50°C) and placed in room
618 temperature distilled water for 15 to 30 minutes. Next, the slides were fixed in 5% sodium
619 thiosulfat pentahydrat for 30 seconds. Slides were dehydrated in an alcohol series and
620 coverslipped with permount. The tissue for a subset of animals used for electrophysiological
621 experiments were processed for TIMM staining and subsequently stained with cresyl violet to
622 facilitate tetrode tracking [74]. For TIMM scoring, the scorer was blinded to condition and scored

623 the extent of mossy fiber sprouting according to the criteria described in [75]. Every sixth section
624 through the dorsal dentate gyrus was given a TIMM score. Sections with no or only occasional
625 supragranular mossy fiber-like staining were scored 0. Sections with scattered mossy fiber-like
626 staining above all parts of the granular layer were given a score of 1. Sections that exhibited
627 either patches of heavy mossy fiber-like staining interspersed with regions of sparser staining or
628 a continuous band of staining intermediate in intensity between sections scored 1 and 3 were
629 given a score of 2. Finally, sections with a dense, continuous band of supragranular mossy fiber-
630 like staining were assigned a score of 3. For analysis, the worst score was selected to represent
631 the maximum extent of sprouting that was observed in a given rat.

632 **Statistics**

633 For each statistical comparison, normality was assessed with Lilliefors test and either
634 parametric or non-parametric tests were chosen accordingly. Multiple comparisons were made
635 with Tukey Kramer post-hoc tests. Throughout the text values are presented as mean ± S.E.M.
636 or median and inter-quartile interval.

637 **FIGURE LEGENDS**

638 **Figure 1. Dentate circuit reorganization and dentate-dependent memory impairment after**
639 **kainic acid treatment. A,** Coronal sections of hippocampi from two KA-treated rats with
640 different degrees of axonal sprouting. Timm stains label zinc concentration black, which is
641 selectively dense in the mossy fiber axons of dentate granule neurons. Magnified images to the
642 right are selected from the area defined by the black boxes centered in the hilar region of the
643 dentate gyrus in the images to the left. Top row, minor sprouting (Timm score 1). Bottom row,
644 intermediate sprouting (Timm score 2). Arrows indicate an example area of sprouting in the
645 inner molecular layer. See Figure S1 for more examples. Scale bars = 250 μm. DG: dentate
646 gyrus; GCL: granule cell layer. **B,** Representative coronal sections of the dentate hilar region
647 from a control rat (top), KA-treated rat without seizures (middle) and a KA-treated rat with
648 seizures (bottom). Somatostatin positive (SST+) neurons are visualized using cell type specific
649 immunohistochemistry. Magnified images to the right are selected from the area defined by
650 the black boxes. (Right) Examples of more abundant SST+ interneurons in the hilus (H) of
651 control rats compared to both KA-treated conditions. **C,** Timm scores indicating degree of
652 mossy fiber sprouting for all rats from each group. Each circle is the average score from one rat.
653 KA-treated rats with seizures have the most extensive mossy fiber sprouting as indicated by
654 significantly higher TIMM scores compared to control rats and KA-treated rats without seizures.
655 **D,** The number of SST+ interneurons in the dorsal hilus is significantly higher in control rats
656 compared to KA-treated rats with and without seizures. Each circle is the average across
657 sections from a single rat. **E**, (Left) Schematic of the dentate-dependent discrimination memory
658 task on an 8-arm radial maze. A single arm is baited with a reward, and two arms are available

659 to the animal, the baited arm and one of the two adjacent arms. The maze was in a small room
660 with distinct distal cues. **F,** The number of trials for rats to preferentially enter the rewarded
661 arm compared to adjacent non-rewarded arms (criterion: 2 of 3 days with ≥90% rewarded
662 trials) by groups (control, KA-treated, and dentate lesioned animals). KA-treated rats with and
663 without seizures are combined, as there were no significant differences between these groups.
664 Ctrl, control; KA, kainic acid treated; seiz, seizures.

665 **Figure S1. Range of TIMM scores observed in KA-treated rats.** (Left) Four images from four
666 different rats, each of which were scored with progressively higher TIMM scores (0-3, top left
667 corner), a measure of the degree of mossy fiber sprouting (see Methods for details on scoring
668 procedure). Sections with no or only occasional supragranular mossy fiber staining were scored
669 0. Sections with scattered mossy fiber staining above all parts of the granular layer were given a
670 score of 1. Sections that exhibited either patches of heavy mossy fiber staining interspersed
671 with regions of sparser staining or a continuous band of staining intermediate in intensity were
672 given a score of 2. Finally, sections with a dense, continuous band of supragranular mossy fiber
673 staining were assigned a score of 3. (Right) Magnified images from the area defined by white
674 boxes in the sections to the left. The magnified area spans the granule cell layer and inner
675 molecular layer (IML). A higher TIMM score reflects a more substantial reorganization of the
676 mossy fibers, including sprouting into regions where axons and terminals are typically not
677 found, such as the IML. For example, the bottom image with the highest TIMM score of 3 is
678 characterized by extensive black fiber tracks within the IML in comparison to control levels
679 (score of 0). GCL, granule cell layer.

680 **Figure 2. Spatial firing patterns of dentate neurons were less precise in KA-treated rats. A,**
681 Cresyl stained coronal section of the dentate gyrus, from a representative control rat with
682 chronic electrophysiological recordings during behavior. The end of a tetrode positioned within
683 the granule cell layer (GCL) is indicated by a circle (see Methods for anatomical tracking of
684 tetrode locations). Neurons are defined as putative granule neurons when the associated
685 tetrode is confirmed by histology to be in the GCL. Scale bar = 250 µm. **B,** Cumulative
686 distribution functions of peak firing rates of recorded dentate neurons (from control and KA-
687 treated rats). Neurons with peak activity >2 Hz (indicated by black dashed line) were considered
688 active. **C,** The average rate of active neurons was similar between KA-treated and control rats.
689 **D,** Activity patterns of individual dentate neurons (10 per group) during 10 min random foraging
690 in a square environment. For each dentate neuron, the spatial information (blue number on top
691 of map) and peak firing rate (black number on bottom of map) were calculated. For each group
692 (control, left; KA-treated, right), the top row comprises rate maps from neurons with the
693 highest spatial information and the bottom row comprises rate maps from neurons with the
694 lowest spatial information. **E,** Firing patterns of dentate neurons carried significantly less spatial
695 information in KA-treated compared to control rats**.** Rate maps of KA-treated dentate neurons
696 contained significantly higher spatial non-selectivity compared to control rats – revealing that
697 spikes were more spatially dispersed after KA treatment. **F,** Number of place fields of a single
698 dentate cell during one 10-min session in the open field and the average size of each place field
699 did not differ between groups. However, the within field average firing rate was higher in KA-
700 treated compared to control rats. Boxplots show median and quartiles, with whiskers extending

701 to minimum and maximum values. *P* values are reported for rank-sum tests. Ctrl, control; KA,
702 kainic acid treated.

703 **Figure S2. The spatial firing properties of dentate neurons from KA-treated rats without**
704 **seizures did not differ from rats that had developed epileptic seizures.** No statistical
705 differences were measured in (A) average firing rate, p = 0.4, (B) spatial information, p = 0.77,
706 or (C) spatial non-selectivity, p = 0.62, when comparing neurons from KA-treated rats with or
707 without observed seizure events (KA-treated no seizure: n = 2 rats, n = 13 active dentate
708 neurons; KA-treated seizure: n = 4 rats, n = 17 active dentate neurons). Active neurons are
709 defined as neurons with a peak rate >2 Hz. Statistics: rank-sum test. KA, kainic acid treated.

710 **Figure 3. Dentate network pattern separation is impaired in KA-treated rats through**
711 **reduction in the capacity of the network to perform rate remapping. A,** (Left) Behavioral
712 paradigm. Animals explored a highly familiar open-field arena in which the shape of the arena
713 could be changed from square to circular (four 10-min sessions; two of each shape presented in
714 random order each day). The arena remained in the same place in the room with common
715 visual cues and a shared floor. The activity of dentate neuron populations was recorded
716 throughout the entire behavioral paradigm. (Right) Dentate population activity was compared
717 across the behavioral sessions as indicated. **B,** Rate maps for all four sessions are shown for two
718 dentate neurons per group (left, control; right KA-treated). Only common areas between the
719 square and circle shape were compared (corresponding to the color-coded maps, which fill the
720 size of the square arena, but are inside the stippled line for the circular area). Rate maps are
721 reordered for visual comparison, regardless of their order during the experiment. All maps are
722 scaled to the peak rate across the entire recording sequence (indicated below the leftmost rate

723 map for each cell). Representative dentate neurons show similar activity patterns in repetitions
724 of the same shape environment, indicating that spatial representations are stable. Firing
725 patterns across shapes are more different as expected for pattern separation across distinct
726 environments. **C,** Schematic illustrating how population vector correlations are computed from
727 dentate population activity. Using separate stacks for recorded neurons from control and KA-
728 treated rats, population vectors were calculated for each spatial bin (x,y) in the environment
729 across all neurons (z). Example numeric population vectors (PV) corresponding to the bin
730 indicated by the pink line are shown below each stack. Bins that include firing fields that change
731 between environments (rate or location of firing) will have low correlation. **D,** (Left) Cumulative
732 distribution functions of population vector correlations between pairs of spatial bins
733 (comparisons indicated in A, right). The dentate population activity was well correlated
734 between repetitions in same-shaped environments in both control (light colored line) and KA-
735 treated rats (dark colored line). When comparing population activity between different shaped
736 environments (dashed lines), the control group exhibited strong decorrelation (light colored
737 dots), in comparison to the KA-treated group where a more moderate decorrelation was
738 observed (dark colored dots). (Right) Control neuron populations discriminated more between
739 different-shape comparisons versus same-shape comparisons than populations from KA-
740 treated rats (change in PV correlation was calculated by subtracting each different-shape-PV
741 from the median of the same-shape-PV), indicating stronger pattern separation in control
742 networks. **E,** (Left) Cumulative distribution functions of each neuron's spatial correlations
743 between pairs of firing rate maps (comparisons indicated in A). Same-shape comparisons were
744 more correlated than different-shape comparisons in both groups (KA-treated, control). P

745 values are reported for post-hoc comparison for KA-treated or control between same and
746 different shapes. (Right) Cumulative distribution functions of the rate overlap between pairs of
747 firing fields (comparisons indicated in A). Only the control group demonstrated strong rate-
748 remapping across distinct environments.

749

750 **REFERENCES**


751 1 O'Reilly, R. C. & McClelland, J. L. Hippocampal conjunctive encoding, storage, and recall:
752 avoiding a trade-off. *Hippocampus* **4**, 661-682 (1994). https://doi.org:10.1002/hipo.450040605
753 2 Leutgeb, J. K., Leutgeb, S., Moser, M. B. & Moser, E. I. Pattern separation in the dentate gyrus
754 and CA3 of the hippocampus. *Science* **315**, 961-966 (2007).
755 https://doi.org:10.1126/science.1135801
756 3 Josselyn, S. A., Kohler, S. & Frankland, P. W. Finding the engram. *Nat Rev Neurosci* **16**, 521-534
757 (2015). https://doi.org:10.1038/nrn4000
758 4 Neunuebel, J. P. & Knierim, J. J. CA3 retrieves coherent representations from degraded input:
759 direct evidence for CA3 pattern completion and dentate gyrus pattern separation. *Neuron* **81**,
760 416-427 (2014). https://doi.org:10.1016/j.neuron.2013.11.017
761 5 Berron, D. *et al.* Strong Evidence for Pattern Separation in Human Dentate Gyrus. *J Neurosci* **36**,
762 7569-7579 (2016). https://doi.org:10.1523/JNEUROSCI.0518-16.2016
763 6 GoodSmith, D., Lee, H., Neunuebel, J. P., Song, H. & Knierim, J. J. Dentate Gyrus Mossy Cells
764 Share a Role in Pattern Separation with Dentate Granule Cells and Proximal CA3 Pyramidal Cells.
765 *J Neurosci* **39**, 9570-9584 (2019). https://doi.org:10.1523/JNEUROSCI.0940-19.2019
766 7 Woods, N. I. *et al.* The Dentate Gyrus Classifies Cortical Representations of Learned Stimuli.
767 *Neuron* **107**, 173-184 e176 (2020). https://doi.org:10.1016/j.neuron.2020.04.002
768 8 Bakker, A., Kirwan, C. B., Miller, M. & Stark, C. E. Pattern separation in the human hippocampal
769 CA3 and dentate gyrus. *Science* **319**, 1640-1642 (2008).
770 https://doi.org:10.1126/science.1152882
771 9 Yassa, M. A. & Stark, C. E. Pattern separation in the hippocampus. *Trends Neurosci* **34**, 515-525
772 (2011). https://doi.org:10.1016/j.tins.2011.06.006
773 10 Amaral, D. G., Scharfman, H. E. & Lavenex, P. The dentate gyrus: fundamental neuroanatomical
774 organization (dentate gyrus for dummies). *Prog Brain Res* **163**, 3-22 (2007).
775 https://doi.org:10.1016/S0079-6123(07)63001-5
776 11 Kesner, R. P. An analysis of the dentate gyrus function. *Behav Brain Res* **254**, 1-7 (2013).
777 https://doi.org:10.1016/j.bbr.2013.01.012
778 12 Marr, D. Simple Memory - Theory for Archicortex. *Philos T Roy Soc B* **262**, 23-& (1971).
779 https://doi.org:DOI 10.1098/rstb.1971.0078
780 13 Chawla, M. K. *et al.* Sparse, environmentally selective expression of Arc RNA in the upper blade
781 of the rodent fascia dentata by brief spatial experience. *Hippocampus* **15**, 579-586 (2005).
782 https://doi.org:10.1002/hipo.20091

14 Piatti, V. C., Ewell, L. A. & Leutgeb, J. K. Neurogenesis in the dentate gyrus: carrying the message or dictating the tone. *Front Neurosci* **7**, 50 (2013). https://doi.org:10.3389/fnins.2013.00050

15 Erwin, S. R. *et al.* A Sparse, Spatially Biased Subtype of Mature Granule Cell Dominates Recruitment in Hippocampal-Associated Behaviors. *Cell Rep* **31**, 107551 (2020). https://doi.org:10.1016/j.celrep.2020.107551

16 Patton, P. E. & McNaughton, B. Connection matrix of the hippocampal formation: I. The dentate gyrus. *Hippocampus* **5**, 245-286 (1995). https://doi.org:10.1002/hipo.450050402

17 Ewell, L. A. & Jones, M. V. Frequency-tuned distribution of inhibition in the dentate gyrus. *J Neurosci* **30**, 12597-12607 (2010). https://doi.org:10.1523/JNEUROSCI.1854-10.2010

18 Braganza, O., Mueller-Komorowska, D., Kelly, T. & Beck, H. Quantitative properties of a feedback circuit predict frequency-dependent pattern separation. *Elife* **9** (2020). https://doi.org:10.7554/eLife.53148

19 Rolls, E. T. Pattern separation, completion, and categorisation in the hippocampus and neocortex. *Neurobiol Learn Mem* **129**, 4-28 (2016). https://doi.org:10.1016/j.nlm.2015.07.008

20 van Dijk, M. T. & Fenton, A. A. On How the Dentate Gyrus Contributes to Memory Discrimination. *Neuron* **98**, 832-845 e835 (2018). https://doi.org:10.1016/j.neuron.2018.04.018

21 Leutgeb, S. *et al.* Independent codes for spatial and episodic memory in hippocampal neuronal ensembles. *Science* **309**, 619-623 (2005). https://doi.org:10.1126/science.1114037

22 Colgin, L. L., Moser, E. I. & Moser, M. B. Understanding memory through hippocampal remapping. *Trends Neurosci* **31**, 469-477 (2008). https://doi.org:10.1016/j.tins.2008.06.008

23 McAvoy, K., Besnard, A. & Sahay, A. Adult hippocampal neurogenesis and pattern separation in DG: a role for feedback inhibition in modulating sparseness to govern population-based coding. *Front Syst Neurosci* **9**, 120 (2015). https://doi.org:10.3389/fnsys.2015.00120

24 Yim, M. Y., Hanuschkin, A. & Wolfart, J. Intrinsic rescaling of granule cells restores pattern separation ability of a dentate gyrus network model during epileptic hyperexcitability. *Hippocampus* **25**, 297-308 (2015). https://doi.org:10.1002/hipo.22373

25 Kahn, J. B., Port, R. G., Yue, C., Takano, H. & Coulter, D. A. Circuit-based interventions in the dentate gyrus rescue epilepsy-associated cognitive dysfunction. *Brain* **142**, 2705-2721 (2019). https://doi.org:10.1093/brain/awz209

26 Madar, A. D., Ewell, L. A. & Jones, M. V. Pattern separation of spiketrains in hippocampal neurons. *Sci Rep* **9**, 5282 (2019). https://doi.org:10.1038/s41598-019-41503-8

27 Lalani, S. J. *et al.* Impaired Behavioral Pattern Separation in Refractory Temporal Lobe Epilepsy and Mild Cognitive Impairment. *J Int Neuropsychol Soc*, 1-13 (2021). https://doi.org:10.1017/S1355617721000734

28 Madar, A. D. *et al.* Deficits in Behavioral and Neuronal Pattern Separation in Temporal Lobe Epilepsy. *J Neurosci* **41**, 9669-9686 (2021). https://doi.org:10.1523/JNEUROSCI.2439-20.2021

29 Buckmaster, P. S. & Dudek, F. E. Network properties of the dentate gyrus in epileptic rats with hilar neuron loss and granule cell axon reorganization. *J Neurophysiol* **77**, 2685-2696 (1997). https://doi.org:10.1152/jn.1997.77.5.2685

30 Buckmaster, P. S. & Dudek, F. E. Neuron loss, granule cell axon reorganization, and functional changes in the dentate gyrus of epileptic kainate-treated rats. *Journal of Comparative Neurology* **385**, 385-404 (1997).

31 Buckmaster, P. S. & Dudek, F. E. In vivo intracellular analysis of granule cell axon reorganization in epileptic rats. *J Neurophysiol* **81**, 712-721 (1999). https://doi.org:10.1152/jn.1999.81.2.712

32 Bragin, A., Benassi, S. K., Kheiri, F. & Engel, J., Jr. Further evidence that pathologic high-frequency oscillations are bursts of population spikes derived from recordings of identified cells in dentate gyrus. *Epilepsia* **52**, 45-52 (2011). https://doi.org:10.1111/j.1528-1167.2010.02896.x

33 Houser, C. R. & Esclapez, M. Vulnerability and plasticity of the GABA system in the pilocarpine model of spontaneous recurrent seizures. *Epilepsy Res* **26**, 207-218 (1996). https://doi.org:Doi 10.1016/S0920-1211(96)00054-X

34 Zhang, W. *et al.* Surviving hilar somatostatin interneurons enlarge, sprout axons, and form new synapses with granule cells in a mouse model of temporal lobe epilepsy. *J Neurosci* **29**, 14247-14256 (2009). https://doi.org:10.1523/JNEUROSCI.3842-09.2009

35 Kobayashi, M. & Buckmaster, P. S. Reduced inhibition of dentate granule cells in a model of temporal lobe epilepsy. *J Neurosci* **23**, 2440-2452 (2003).

36 Lynch, M., Sayin, U., Golarai, G. & Sutula, T. NMDA receptor-dependent plasticity of granule cell spiking in the dentate gyrus of normal and epileptic rats. *J Neurophysiol* **84**, 2868-2879 (2000). https://doi.org:10.1152/jn.2000.84.6.2868

37 Kelly, T. & Beck, H. Functional properties of granule cells with hilar basal dendrites in the epileptic dentate gyrus. *Epilepsia* **58**, 160-171 (2017). https://doi.org:10.1111/epi.13605

38 Dengler, C. G., Yue, C., Takano, H. & Coulter, D. A. Massively augmented hippocampal dentate granule cell activation accompanies epilepsy development. *Sci Rep* **7**, 42090 (2017). https://doi.org:10.1038/srep42090

39 Krook-Magnuson, E. *et al.* In vivo evaluation of the dentate gate theory in epilepsy. *J Physiol* **593**, 2379-2388 (2015). https://doi.org:10.1113/JP270056

40 Gilbert, P. E., Kesner, R. P. & Lee, I. Dissociating hippocampal subregions: double dissociation between dentate gyrus and CA1. *Hippocampus* **11**, 626-636 (2001). https://doi.org:10.1002/hipo.1077

41 Lee, C. H. & Lee, I. Impairment of Pattern Separation of Ambiguous Scenes by Single Units in the CA3 in the Absence of the Dentate Gyrus. *J Neurosci* **40**, 3576-3590 (2020). https://doi.org:10.1523/JNEUROSCI.2596-19.2020

42 Morris, A. M., Churchwell, J. C., Kesner, R. P. & Gilbert, P. E. Selective lesions of the dentate gyrus produce disruptions in place learning for adjacent spatial locations. *Neurobiol Learn Mem* **97**, 326-331 (2012). https://doi.org:10.1016/j.nlm.2012.02.005

43 McHugh, T. J. *et al.* Dentate gyrus NMDA receptors mediate rapid pattern separation in the hippocampal network. *Science* **317**, 94-99 (2007). https://doi.org:10.1126/science.1140263

44 Leutgeb, J. K. *et al.* Progressive transformation of hippocampal neuronal representations in "morphed" environments. *Neuron* **48**, 345-358 (2005). https://doi.org:10.1016/j.neuron.2005.09.007

45 Shuman, T. *et al.* Breakdown of spatial coding and interneuron synchronization in epileptic mice. *Nat Neurosci* **23**, 229-238 (2020). https://doi.org:10.1038/s41593-019-0559-0

46 Dinocourt, C., Petanjek, Z., Freund, T. F., Ben-Ari, Y. & Esclapez, M. Loss of interneurons innervating pyramidal cell dendrites and axon initial segments in the CA1 region of the hippocampus following pilocarpine-induced seizures. *J Comp Neurol* **459**, 407-425 (2003). https://doi.org:10.1002/cne.10622

47 Bouilleret, V., Loup, F., Kiener, T., Marescaux, C. & Fritschy, J. M. Early loss of interneurons and delayed subunit-specific changes in GABA(A)-receptor expression in a mouse model of mesial temporal lobe epilepsy. *Hippocampus* **10**, 305-324 (2000). https://doi.org:10.1002/1098-1063(2000)10:3<305::AID-HIPO11>3.0.CO;2-I

48 Hofmann, G., Balgooyen, L., Mattis, J., Deisseroth, K. & Buckmaster, P. S. Hilar somatostatin interneuron loss reduces dentate gyrus inhibition in a mouse model of temporal lobe epilepsy. *Epilepsia* **57**, 977-983 (2016). https://doi.org:10.1111/epi.13376

49 McKenzie, S. *et al.* Preexisting hippocampal network dynamics constrain optogenetically induced place fields. *Neuron* **109**, 1040-1054 e1047 (2021). https://doi.org:10.1016/j.neuron.2021.01.011

50 Rolotti, S. V. *et al.* Local feedback inhibition tightly controls rapid formation of hippocampal place fields. *Neuron* **110**, 783-794 e786 (2022). https://doi.org:10.1016/j.neuron.2021.12.003

51 Royer, S. *et al.* Control of timing, rate and bursts of hippocampal place cells by dendritic and somatic inhibition. *Nat Neurosci* **15**, 769-775 (2012). https://doi.org:10.1038/nn.3077

52 Chavlis, S., Petrantonakis, P. C. & Poirazi, P. Dendrites of dentate gyrus granule cells contribute to pattern separation by controlling sparsity. *Hippocampus* **27**, 89-110 (2017). https://doi.org:10.1002/hipo.22675

53 Galloni, A. R., Samadzelkava, A., Hiremath, K., Oumnov, R. & Milstein, A. D. Recurrent Excitatory Feedback From Mossy Cells Enhances Sparsity and Pattern Separation in the Dentate Gyrus via Indirect Feedback Inhibition. *Front Comput Neurosci* **16**, 826278 (2022). https://doi.org:10.3389/fncom.2022.826278

54 Freund, T. F. & Buzsaki, G. Interneurons of the hippocampus. *Hippocampus* **6**, 347-470 (1996). https://doi.org:10.1002/(SICI)1098-1063(1996)6:4<347::AID-HIPO1>3.0.CO;2-I

55 Witter, M. P. Organization of the entorhinal-hippocampal system: a review of current anatomical data. *Hippocampus* **3 Spec No**, 33-44 (1993).

56 Hargreaves, E. L., Rao, G., Lee, I. & Knierim, J. J. Major dissociation between medial and lateral entorhinal input to dorsal hippocampus. *Science* **308**, 1792-1794 (2005). https://doi.org:10.1126/science.1110449

57 Tsao, A. *et al.* Integrating time from experience in the lateral entorhinal cortex. *Nature* **561**, 57-62 (2018). https://doi.org:10.1038/s41586-018-0459-6

58 Lu, L. *et al.* Impaired hippocampal rate coding after lesions of the lateral entorhinal cortex. *Nat Neurosci* **16**, 1085-1093 (2013). https://doi.org:10.1038/nn.3462

59 Santhakumar, V., Aradi, I. & Soltesz, I. Role of mossy fiber sprouting and mossy cell loss in hyperexcitability: a network model of the dentate gyrus incorporating cell types and axonal topography. *J Neurophysiol* **93**, 437-453 (2005). https://doi.org:10.1152/jn.00777.2004

60 Liu, X. *et al.* Seizure-induced changes in place cell physiology: relationship to spatial memory. *J Neurosci* **23**, 11505-11515 (2003). https://doi.org:10.1523/JNEUROSCI.23-37-11505.2003

61 Ewell, L. A., Fischer, K. B., Leibold, C., Leutgeb, S. & Leutgeb, J. K. The impact of pathological high-frequency oscillations on hippocampal network activity in rats with chronic epilepsy. *Elife* **8** (2019). https://doi.org:10.7554/eLife.42148

62 Hunt, R. F., Girskis, K. M., Rubenstein, J. L., Alvarez-Buylla, A. & Baraban, S. C. GABA progenitors grafted into the adult epileptic brain control seizures and abnormal behavior. *Nat Neurosci* **16**, 692-697 (2013). https://doi.org:10.1038/nn.3392

63 Zhu, B., Eom, J. & Hunt, R. F. Transplanted interneurons improve memory precision after traumatic brain injury. *Nat Commun* **10**, 5156 (2019). https://doi.org:10.1038/s41467-019-13170-w

64 Ewell, L. A. *et al.* Brain State Is a Major Factor in Preseizure Hippocampal Network Activity and Influences Success of Seizure Intervention. *J Neurosci* **35**, 15635-15648 (2015). https://doi.org:10.1523/JNEUROSCI.5112-14.2015

65 Hellier, J. L., Patrylo, P. R., Buckmaster, P. S. & Dudek, F. E. Recurrent spontaneous motor seizures after repeated low-dose systemic treatment with kainate: assessment of a rat model of temporal lobe epilepsy. *Epilepsy Res* **31**, 73-84 (1998). https://doi.org:Doi 10.1016/S0920-1211(98)00017-5

66 Racine, R. J. Modification of seizure activity by electrical stimulation. II. Motor seizure. *Electroencephalogr Clin Neurophysiol* **32**, 281-294 (1972). https://doi.org:10.1016/0013-4694(72)90177-0

67 Snyder, J. S. *et al.* A Transgenic Rat for Specifically Inhibiting Adult Neurogenesis. *eNeuro* **3** (2016). https://doi.org:10.1523/ENEURO.0064-16.2016

68 McNaughton, B. L. Neuronal 'Ensemble' Recording and the Search for the Cell Assembly: A Personal History. *Hippocampus* **35**, e23669 (2025). https://doi.org:10.1002/hipo.23669

69 Sasaki, T. *et al.* Dentate network activity is necessary for spatial working memory by supporting CA3 sharp-wave ripple generation and prospective firing of CA3 neurons. *Nat Neurosci* **21**, 258-269 (2018). https://doi.org:10.1038/s41593-017-0061-5

70 Walsh, T. J., Schulz, D. W., Tilson, H. A. & Schmechel, D. E. Colchicine-induced granule cell loss in rat hippocampus: selective behavioral and histological alterations. *Brain Res* **398**, 23-36 (1986). https://doi.org:10.1016/0006-8993(86)91246-1

71 Goldschmidt, R. B. & Steward, O. Preferential neurotoxicity of colchicine for granule cells of the dentate gyrus of the adult rat. *Proc Natl Acad Sci U S A* **77**, 3047-3051 (1980). https://doi.org:10.1073/pnas.77.5.3047

72 Mankin, E. A. *et al.* Neuronal code for extended time in the hippocampus. *Proc Natl Acad Sci U S A* **109**, 19462-19467 (2012). https://doi.org:10.1073/pnas.1214107109

73 Skaggs WE, M. B., Gothard KM, Markus EJ. . *An information-theoretic approach to deciphering the hippocampal code*. (1993).

74 Mankin, E. A., Diehl, G. W., Sparks, F. T., Leutgeb, S. & Leutgeb, J. K. Hippocampal CA2 activity patterns change over time to a larger extent than between spatial contexts. *Neuron* **85**, 190-201 (2015). https://doi.org:10.1016/j.neuron.2014.12.001

75 Tauck, D. L. & Nadler, J. V. Evidence of functional mossy fiber sprouting in hippocampal formation of kainic acid-treated rats. *J Neurosci* **5**, 1016-1022 (1985).

Figure 1

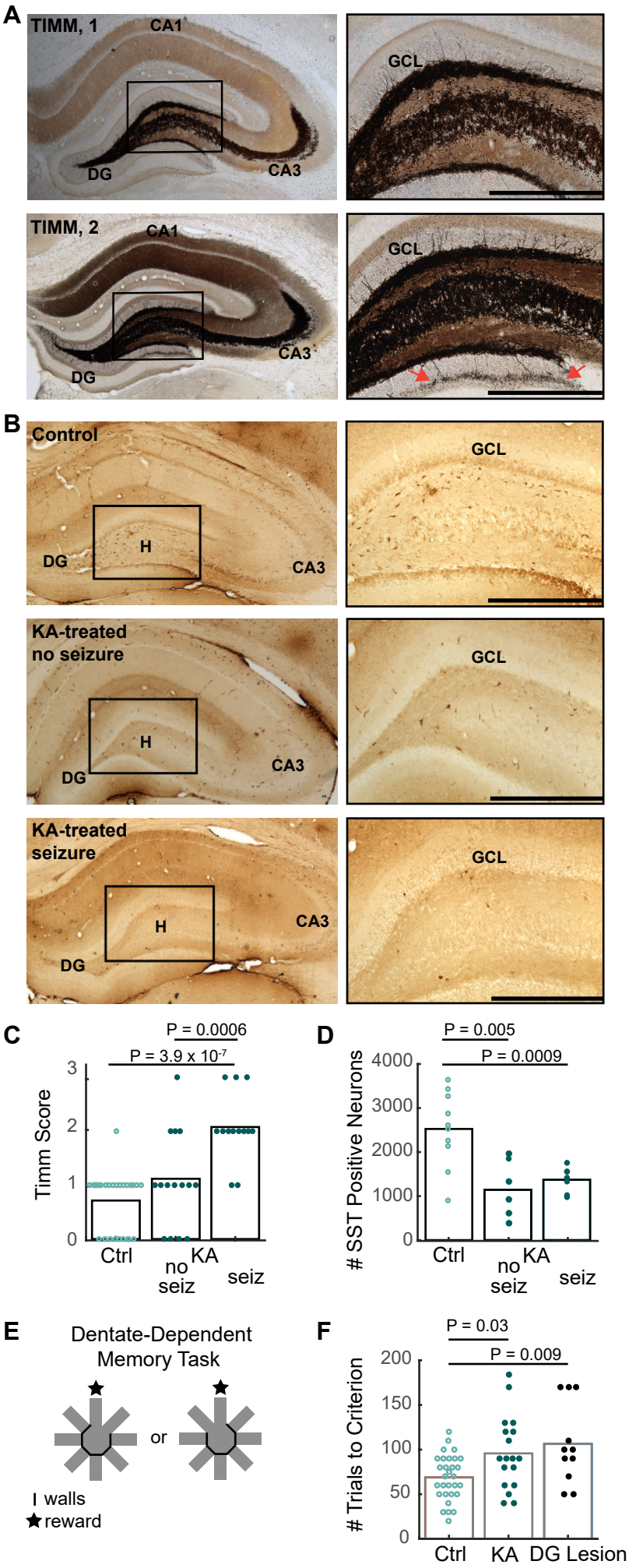
A
TIMM, 1
CA1
DG
CA3
GCL
TIMM, 2
CA1
DG
CA3
GCL
B
Control
DG
H
CA3
GCL
KA-treated
no seizure
DG
H
CA3
GCL
KA-treated
seizure
DG
H
CA3
GCL
C
P = 0.0006
P = 3.9 x 10-7
Timm Score
0
1
2
3
Ctrl
no seiz
KA seiz
D
P = 0.005
P = 0.0009
# SST Positive Neurons
0
1000
2000
3000
4000
Ctrl
no seiz
KA seiz
E
Dentate-Dependent
Memory Task
or
walls
reward
F
P = 0.03
P = 0.009
# Trials to Criterion
0
50
100
150
200
Ctrl
KA
DG Lesion

**Figure S1**

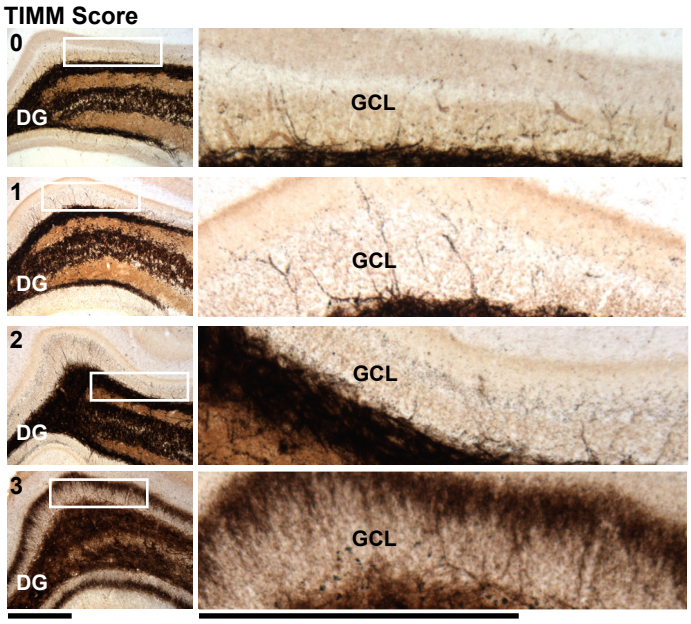

**Figure 2**

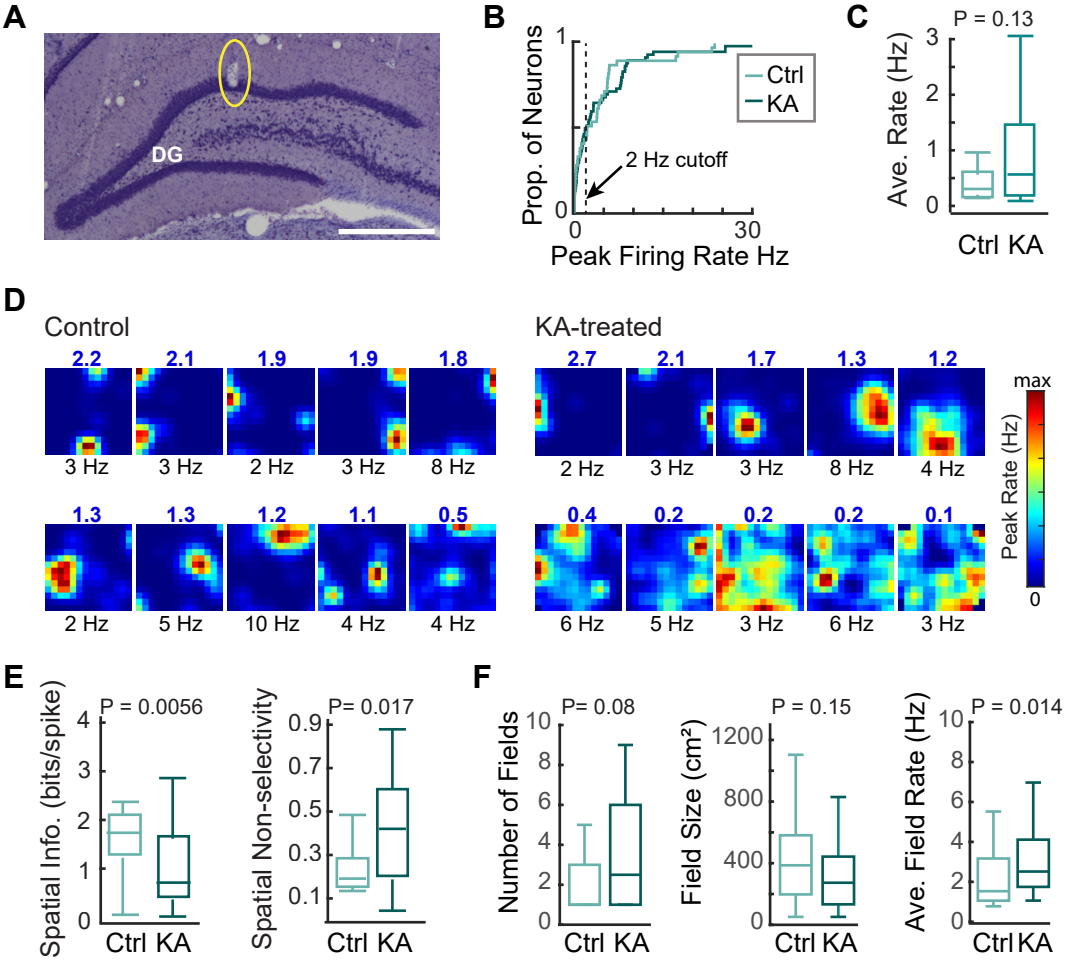
A
DG
B
Prop. of Neurons
Peak Firing Rate Hz
2 Hz cutoff
Ctrl
KA
C
P = 0.13
Ave. Rate (Hz)
Ctrl KA
D
Control
KA-treated
2.2 2.1 1.9 1.9 1.8
3 Hz 3 Hz 2 Hz 3 Hz 8 Hz
1.3 1.3 1.2 1.1 0.5
2 Hz 5 Hz 10 Hz 4 Hz 4 Hz
2.7 2.1 1.7 1.3 1.2
2 Hz 3 Hz 3 Hz 8 Hz 4 Hz
0.4 0.2 0.2 0.2 0.1
6 Hz 5 Hz 3 Hz 6 Hz 3 Hz
max
Peak Rate (Hz)
0
E
Spatial Info. (bits/spike)
P = 0.0056
Ctrl KA
Spatial Non-selectivity
P= 0.017
Ctrl KA
F
Number of Fields
P= 0.08
Ctrl KA
Field Size (cm²)
P = 0.15
Ctrl KA
Ave. Field Rate (Hz)
P = 0.014
Ctrl KA

**Figure S2**

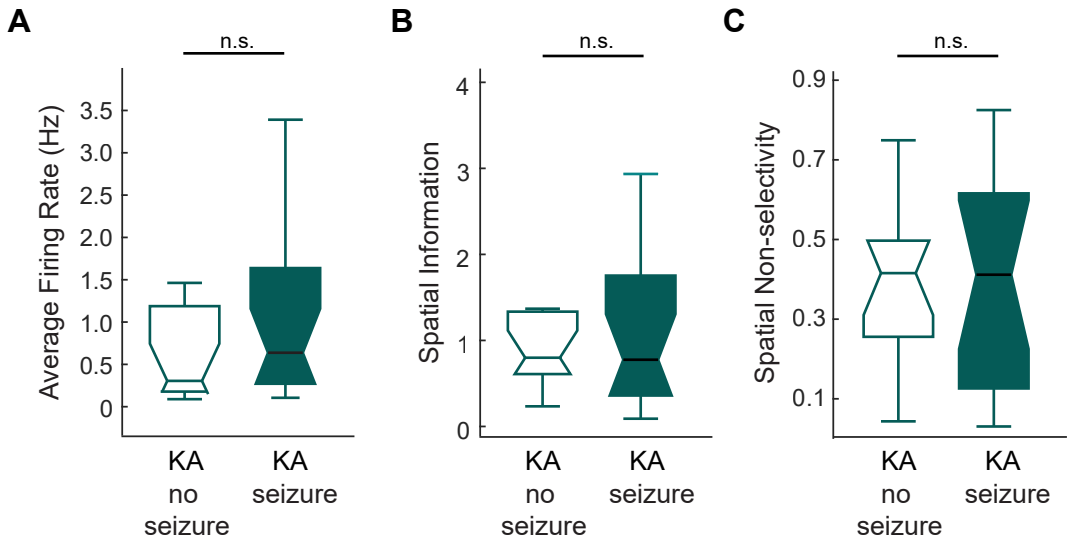
A
n.s.
Average Firing Rate (Hz)
3.5
3.0
2.5
2.0
1.5
1.0
0.5
0
KA no seizure
KA seizure
B
n.s.
Spatial Information
4
3
2
1
0
KA no seizure
KA seizure
C
n.s.
Spatial Non-selectivity
0.9
0.7
0.5
0.3
0.1
KA no seizure
KA seizure

**Figure 3**

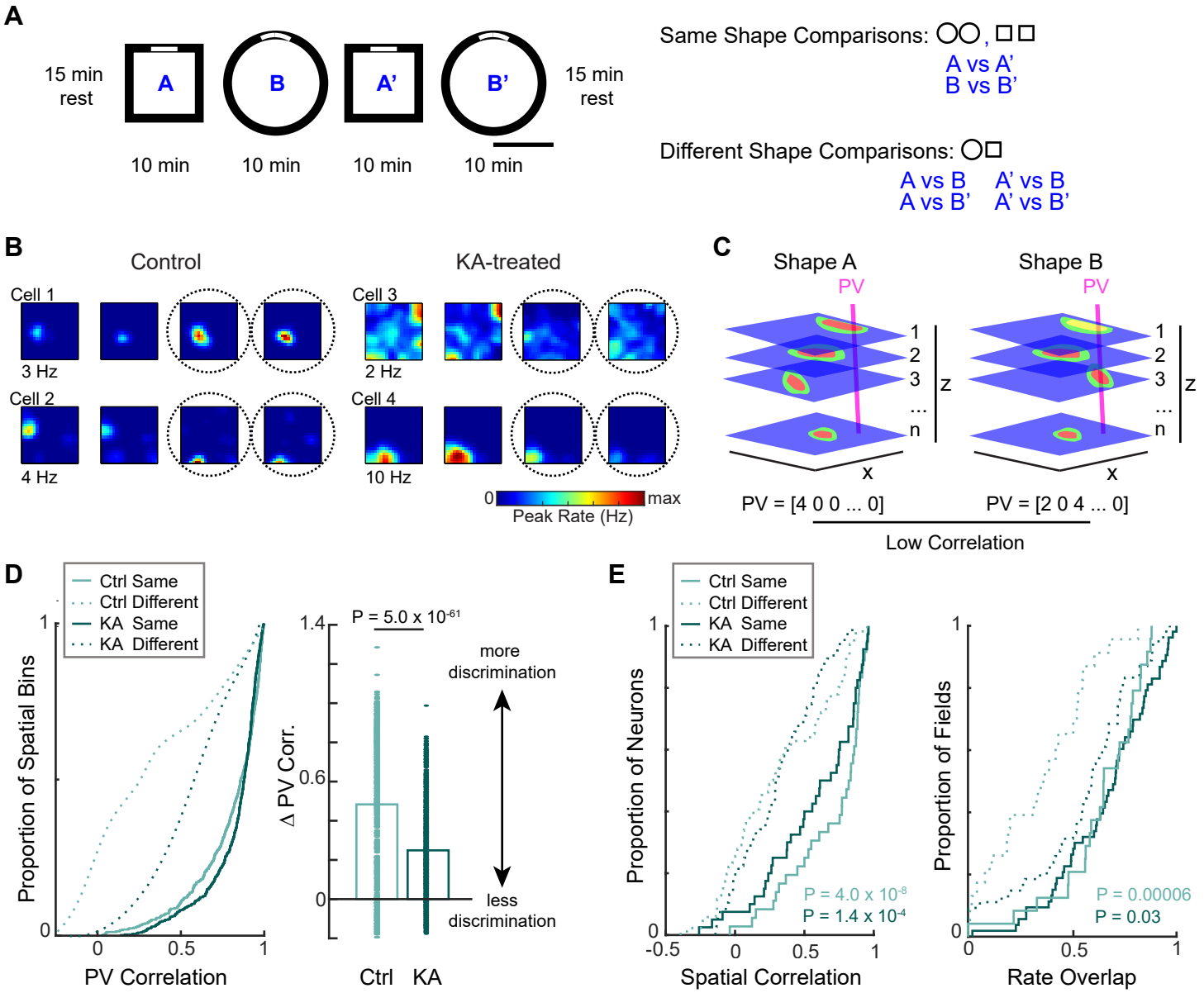
A
15 min rest
A
B
A'
B'
15 min rest
10 min
10 min
10 min
10 min
Same Shape Comparisons:
A vs A'
B vs B'
Different Shape Comparisons:
A vs B
A vs B'
A' vs B
A' vs B'
B
Control
KA-treated
Cell 1
3 Hz
Cell 2
4 Hz
Cell 3
2 Hz
Cell 4
10 Hz
0
max
Peak Rate (Hz)
C
Shape A
Shape B
PV
1
2
3
...
n
z
x
PV = [4 0 0 ... 0]
PV = [2 0 4 ... 0]
Low Correlation
D
Ctrl Same
Ctrl Different
KA Same
KA Different
Proportion of Spatial Bins
PV Correlation
P = 5.0 x 10-61
Δ PV Corr.
more discrimination
less discrimination
Ctrl
KA
E
Proportion of Neurons
Spatial Correlation
P = 4.0 x 10-8
P = 1.4 x 10-4
Proportion of Fields
Rate Overlap
P = 0.00006
P = 0.03